

High-Mobility Electron Conduction in Oxynitride: Anatase TaON

Atsushi Suzuki,^{†,‡} Yasushi Hirose,^{*,†,‡,§} Daichi Oka,^{†,‡} Shoichiro Nakao,^{‡,§} Tomoteru Fukumura,^{†,‡,§} Satoshi Ishii,^{||} Kimikazu Sasa,^{||} Hiroyuki Matsuzaki,[⊥] and Tetsuya Hasegawa^{†,‡,§}

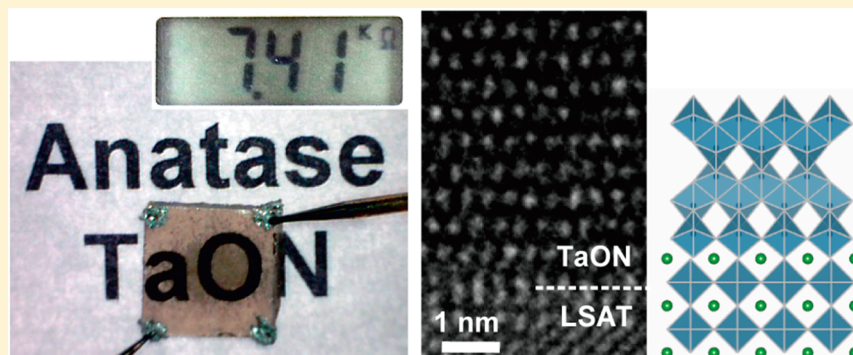
[†]Department of Chemistry, School of Science, The University of Tokyo, 7-3-1 Hongo, Bunkyo-ku, Tokyo 113-0033, Japan

[‡]Kanagawa Academy of Science and Technology, 3-2-1 Sakado, Takatsu-ku, Kawasaki 213-0012, Japan

[§]CREST, Japan Science and Technology Agency, 7-3-1 Hongo, Bunkyo-ku, Tokyo 113-0033, Japan

^{||}Tandem Accelerator Complex, University of Tsukuba, 1-1-1 Tennodai, Tsukuba 305-8577, Japan

[⊥]Department of Nuclear Engineering and Management, School of Engineering, The University of Tokyo, 2-11-16 Yayoi, Bunkyo-ku, Tokyo 113-0032, Japan



ABSTRACT: We report on a new route for synthesizing metastable anatase tantalum oxynitride (TaON) in thin film form on lattice-matched $(\text{LaAlO}_3)_{0.3} \cdot (\text{SrAl}_{0.5}\text{Ta}_{0.5}\text{O}_3)_{0.7}$ (LSAT) single crystals by using nitrogen plasma assisted pulsed laser deposition. Epitaxial stress from the substrate stabilized the anatase structure without the need for doping an impurity, such as Sc or Mg, which is required in conventional bulk synthesis by ammonolysis. X-ray diffraction measurements and cross-sectional transmission electron microscope (TEM) observations demonstrated the growth of phase-pure anatase TaON thin films with the epitaxial relationships $(001)_{\text{TaON}} \parallel (001)_{\text{LSAT}}$ and $[100]_{\text{TaON}} \parallel [100]_{\text{LSAT}}$. A high growth temperature (≥ 750 °C) and a balanced supply of oxygen and nitrogen are crucial for obtaining high-quality anatase TaON thin films. The films grown at 800 °C exhibited good *n*-type conduction with a resistivity of $\sim 1 \times 10^{-2}$ Ω cm. The source of the carrier electrons was likely anion vacancies. The Hall mobility of anatase TaON (~ 17 cm² V⁻¹ s⁻¹ at 300 K) is comparably high to that of anatase TiO₂, which is a well-known oxide semiconductor with the same crystal structure and *d*⁰ electronic configuration. The bandgap and refractive index of anatase TaON thin films were 2.37 eV and approximately 3.0, respectively, in the visible region.

KEYWORDS: tantalum oxynitride, anatase, thin film, semiconductor, high mobility

INTRODUCTION

In the past decade, transition metal oxynitrides have attracted much attention as nontoxic pigments¹ or photocatalysts^{2,3} due to their optical bandgap (E_g) in the visible light region and their band alignment, making them suitable for photocatalytic water splitting. In contrast to the extensive studies carried out on the optical and photochemical properties of oxynitrides, less attention has been paid to their electrical properties, mainly because of the difficulty in obtaining single crystalline or densely sintered samples: oxynitrides start to decompose at much lower temperature than their melting point. Considering the diverse progress made in oxide- and nitride-based electronics, transition metal oxynitrides exhibit attractive electrical properties.⁴ Recently, in fact, novel electrical functionalities were found in oxynitrides, as exemplified by high electron mobility in amorphous ZnO_xN_y ^{5,6} and carrier

type tunability and colossal magnetoresistance in $\text{EuWO}_{1+x}\text{N}_{2-x}$ ⁷

In this study, we focused on anatase-type tantalum oxynitride (TaON) from the viewpoint of electronics application, because its crystal structure and cation electronic configuration (*d*⁰) are identical to those of anatase TiO₂, which is a well-established *n*-type oxide semiconductor. Anatase is a very rare structure composed of edge-sharing metal-O₆ octahedra. Anatase TiO₂ is characterized by high Hall mobility (~ 17 cm² V⁻¹ s⁻¹ at 300 K and over 500 cm² V⁻¹ s⁻¹ at ~ 50 K)⁸ and wide controllability of the carrier density, from insulator to degenerated semiconductor, by chemical doping (Nb⁵⁺ (ref 9), Ta⁵⁺ (ref 10),

Received: August 12, 2013

Revised: December 10, 2013

Published: December 16, 2013

W^{6+} (ref 11), F^- (ref 12), or oxygen vacancy¹³). A variety of electronic materials and devices based on anatase TiO_2 have been proposed to date, including a transparent conductor,⁹ a ferromagnetic semiconductor,¹⁴ a thin film transistor,¹⁵ and a resistive random access memory.¹⁶ Thus, it is expected that anatase TaON has the potential to be used as an *n*-type semiconductor with high Hall mobility. Thus far, however, anatase TaON has been synthesized only in polycrystalline fine powder form by nitriding precursor oxides under high-temperature ammonia flow (ammonolysis),^{17,18} similar to other transition metal oxynitrides. Furthermore, because anatase is a metastable polymorph of TaON,^{17–20} substitution of 5–15% of Mg^{2+} or Sc^{3+} for Ta^{5+} , which behaves as an acceptor to trap carrier electrons, is needed to stabilize the anatase structure.^{17,18} These practical factors, i.e., poor electrical connection between randomly oriented grains and high concentration of doped acceptor impurities, hinder investigation of the electrical properties of anatase TaON. Indeed, electrical transport properties of anatase TaON have never been reported.

Here, we present a new synthetic route of anatase TaON, namely, epitaxial growth on a lattice-matched single crystalline substrate, where the epitaxial force from the substrate stabilizes the metastable anatase structure without the need for impurity doping. The undoped TaON thin films obtained with this method showed a single-crystal quality that was hardly affected by grain boundaries, which enabled us to evaluate the transport properties. The anatase TaON thin films grown at 800 °C exhibited good electrical conductivity of $\sim 1 \times 10^{-2} \Omega \text{ cm}$ and a temperature-independent *n*-type carrier density on the order of 10^{19} cm^{-3} , which are characteristic of degenerated semiconductors. The Hall mobility was as high as $17 \text{ cm}^2 \text{ V}^{-1} \text{ s}^{-1}$ at 300 K, which is comparable to that of anatase TiO_2 .

■ EXPERIMENTAL SECTION

Anatase TaON thin films were grown by nitrogen plasma assisted pulsed laser deposition (NPA-PLD) on $(\text{LaAlO}_3)_{0.3}(\text{SrAl}_{0.5}\text{Ta}_{0.5}\text{O}_3)_{0.7}$ (LSAT) (001) single crystalline substrate (cubic, $a/2 = 0.3868 \text{ nm}$) with good lattice matching to the (001)-plane of anatase TaON predicted by a first-principles calculation (tetragonal, $a = 0.392 \text{ nm}$).²⁰ A ceramic Ta_2O_5 target was sintered from Ta_2O_5 powder (99.99% purity) at 1400 °C for 15 h in air. A pulsed laser beam from a KrF excimer laser ($\lambda = 248 \text{ nm}$) was focused onto the Ta_2O_5 target. The fluence and repetition rate of the excimer laser were adjusted to control the deposition rate to 10–16 nm/h. The substrate temperature (T_S), serving as the main growth parameter, was varied from 650 to 800 °C by infrared lamp heating. Deposition was conducted under a partial N_2 gas pressure of $1 \times 10^{-5} \text{ Torr}$, where the supplied N_2 gas was activated into radicals by a radio frequency wave (RF) plasma source (SVT Associates, Model 4.5 in.) with an output power of 250 W. Typical film thicknesses were 30–45 nm, evaluated by a stylus profiler with experimental uncertainty of $\sim 5 \text{ nm}$. Some of the films were successively annealed at 800 °C for 20 min under base pressure ($< 2 \times 10^{-7} \text{ Torr}$) in the growth chamber.

Crystal structures of the films were examined by X-ray diffraction (XRD) measurements using Cu $\text{K}\alpha$ radiation and a four-axis diffractometer (Bruker AXS, d8 discover). Cross-sectional transmission electron microscope (TEM) observation was also performed to ensure the microscopic structure of the film. The TEM specimen was prepared by the focused ion beam microsampling method. The oxygen and nitrogen contents were evaluated by an energy dispersive X-ray spectroscope equipped with a scanning electron microscope (SEM-EDX), within experimental errors of $\sim 10\%$. The electron accelerating voltage was set at 2.5 kV in order to reduce the background signal from the substrate. The nitrogen content was also cross-checked by nuclear reaction analysis (NRA) using a $^{15}\text{N}(p,$

$\alpha\gamma)^{12}\text{C}$ resonance reaction at 898 keV, which included an experimental error of $\sim 20\%$ due to the small sample thickness and instability of the energy of a proton beam. Electrical resistivity (ρ), carrier electron density (n_e), and Hall mobility (μ_H) were determined by the van der Pauw method²¹ with Au/Ti electrodes. The ρ values of highly resistive samples were evaluated by a two-probe method. A physical property measurement system (Quantum Design, model 6000) was used to control the sample temperature between 10 and 300 K and the external magnetic field between –9 and 9 T. Optical constants of the anatase TaON films were determined by spectroscopic ellipsometry (J. A. Woolam, M-2000U) in a spectral range of 1–5 eV. A series of ellipsometric spectra obtained at incident/reflection angles from 50° to 80° with 5° step were analyzed by using a simple model consisting of a single-layer film and a substrate. The dispersion function of the TaON film was modeled as a sum of single Tauc–Lorentz²² and single Lorentz dispersion functions. The optical anisotropy of anatase TaON was ignored in the analysis because isotropic and anisotropic optical models gave almost the same results.

■ RESULTS AND DISCUSSION

Synthesis of Anatase TaON Epitaxial Thin Films.

Anatase TaON thin films were grown by NPA-PLD, where a ceramic Ta_2O_5 target was ablated and reacted with nitrogen radical introduced into the growth chamber. Figure 1a compares θ – 2θ XRD patterns of the TaON films grown on LSAT (001) single crystal substrates at various T_S . As seen from the figure, the crystal growth was quite sensitive to T_S . The films grown at $T_S \geq 750 \text{ }^\circ\text{C}$ showed peaks at $2\theta = \sim 35^\circ$ and $\sim 74^\circ$, which correspond well to the 004 and 008 diffraction of anatase TaON predicted by first-principles calculations,²⁰ namely, $2\theta = 35.5^\circ$ and 75.2° , respectively. Meanwhile, for the film deposited at $T_S \leq 700 \text{ }^\circ\text{C}$, these peaks became weak or even undetectable. We also conducted asymmetrical reflection measurements on the films grown at $T_S \geq 750 \text{ }^\circ\text{C}$ and confirmed the epitaxial relationships $(001)_{\text{TaON}} \parallel (001)_{\text{LSAT}}$ and $[100]_{\text{TaON}} \parallel [100]_{\text{LSAT}}$, as expected from the lattice-matching. The φ -scan plot of the 101 diffraction (Figure 1b) revealed fourfold rotational symmetry, consistent with this epitaxial relationship. The full width at half-maximum (fwhm) value of the φ -scan plot was $\sim 0.6^\circ$, implying the presence of small in-plane twists in the film. We also note that no impurity phases, such as Ta_2O_5 and baddeleyite-TaON, were detected in these measurements.

The film grown at $T_S = 750 \text{ }^\circ\text{C}$ was further investigated by cross-sectional TEM. A low-magnification TEM observation (Figure 2a) revealed a sharp interface between the film and substrate, without intermixing or phase segregation, though planar defects along the {101} planes of anatase TaON, possibly originating from stacking faults, were frequently seen. The fact that the triangular domains were imaged with different contrast may reflect the small in-plane twisting of the crystals mentioned above. High-resolution TEM images (Figures 2b,c) showed a characteristic lattice pattern of the anatase structure, as reported previously for anatase TiO_2 .²³ The electron diffraction pattern (Figure 2d) also verified the (001) growth of anatase TaON. From these results, we concluded that phase-pure anatase TaON was successfully obtained as a consequence of the epitaxial force from the LSAT substrate, without the aid of Mg or Sc doping. The chemical composition of the anatase TaON thin film grown at 750 °C was evaluated as $\text{TaO}_{0.94 \pm 0.09}\text{N}_{1.04 \pm 0.1}$ by using SEM-EDX. The nitrogen content per formula unit determined by NRA was 1.2 ± 0.2 , which is in good agreement with the SEM-EDX results, within the experimental error.

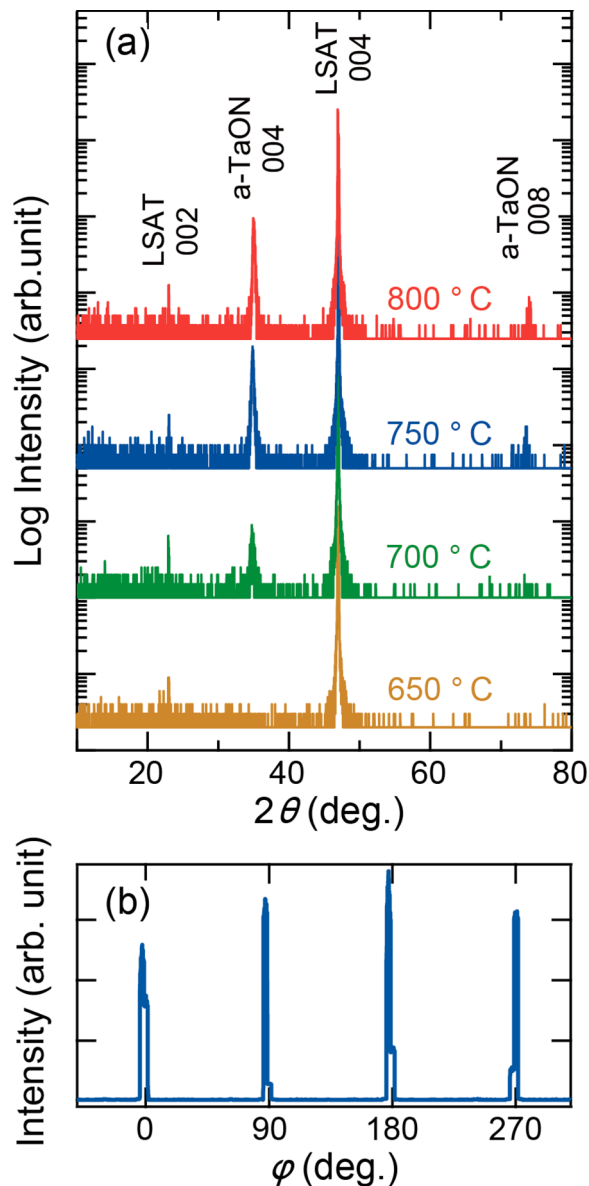


Figure 1. (a) θ - 2θ XRD patterns of the TaON films grown on LSAT substrates at various T_S . “a-TaON” represents anatase TaON. (b) φ -scan plot of 101 diffraction from the anatase TaON film grown at 750 °C. $\varphi = 0^\circ$ was set parallel to the $\langle 100 \rangle$ direction of the LSAT substrate.

Figure 3a shows the rocking curves of the anatase TaON 004 diffraction measured for the films grown at various T_S . Notably, the fwhm value shows a minimum $\sim 0.09^\circ$ at $T_S = 750$ °C; in other words, the best crystallinity was obtained at $T_S = 750$ °C. Another key growth parameter is the film growth rate, which is determined by the ablation rate of the Ta_2O_5 target. At a high ablation rate (high laser fluence or high repetition rate), oxygen was oversupplied from the target compared with the nitrogen radical introduced from the plasma source, resulting in the formation of Ta_2O_5 as a secondary phase (Figure 3b). At $T_S \geq 750$ °C, the optimal deposition rate was found to be 10–16 nm/h. In the following section, we present the physical properties of the phase-pure anatase TaON thin films grown at $T_S \geq 750$ °C.

Electrical Transport Properties of Anatase TaON.

Figure 4a plots ρ values of the anatase TaON films fabricated

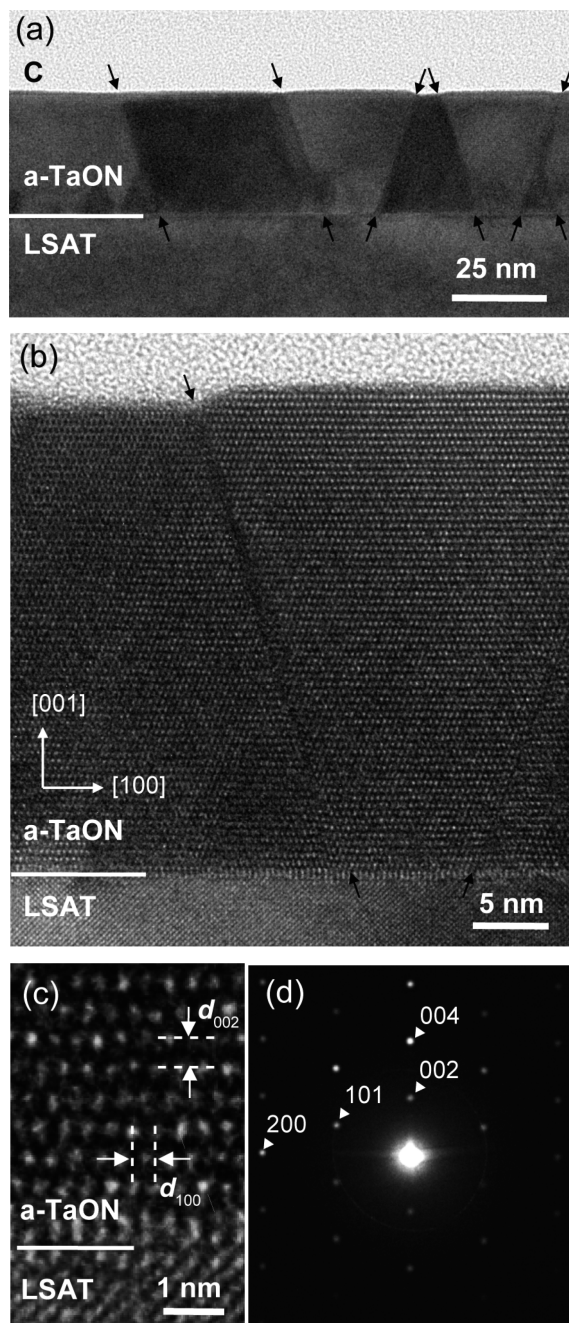


Figure 2. (a, b) Cross-sectional TEM image of the anatase TaON thin film grown at 750 °C, viewed along the $[010]$ zone axis of the LSAT substrate. The arrows indicate planar defects along the $\{101\}$ planes of the anatase TaON. (c) High-resolution image of the same sample. (d) Electron diffraction pattern of the same anatase TaON film. The weak ring pattern originated from the carbon coated on the film.

at $T_S = 750$ and 800 °C as functions of temperature. The former showed a high ρ of 10^2 Ω cm order at 300 K and semiconducting temperature dependence ($d\rho/dT < 0$), whereas the latter showed a 4 orders of magnitude lower ρ at 300 K ($\sim 1 \times 10^{-2}$ Ω cm) and metallic temperature dependence ($d\rho/dT > 0$) down to ~ 100 K. Hall measurements revealed that electrons carried the charges (*n*-type semiconductor). Considering the T_S dependence of ρ and the *n*-type conduction, the carrier electrons might have originated from anion vacancies, whose number would increase at higher T_S , as frequently seen in oxide or nitride semiconductors. We further annealed the

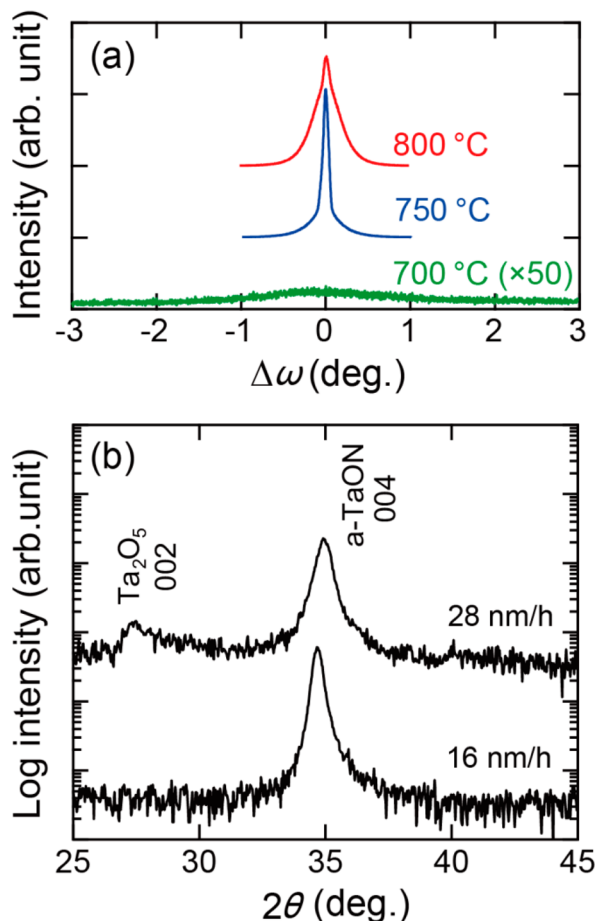


Figure 3. (a) Rocking curves of anatase TaON 004 for the films grown at various T_S . (b) θ - 2θ plots of the anatase TaON thin films deposited at 750 °C with optimal (16 nm/h) and excessively high (28 nm/h) growth rates. The output power of the RF source was set at 300 W for the deposition of the films in (b).

anatase TaON film ($T_S = 750$ °C) in vacuum at 800 °C. As shown in Figure 4a, ρ was substantially reduced by the annealing, and the $\rho-T$ curve of the annealed film was comparable to that of the anatase TaON film grown at $T_S = 800$ °C, supporting the above hypothesis about the carrier source. We note that the number of anion vacancies could not be determined by composition analysis, because the number of vacancies estimated from the carrier density was much lower than the experimental error (~10%). In fact, the chemical composition of the film grown at $T_S = 800$ °C was evaluated as $\text{TaO}_{1.0 \pm 0.1}\text{N}_{1.0 \pm 0.1}$ by SEM-EDX, which agreed well with the film grown at $T_S = 750$ °C, within the experimental error.

Figure 4b,c shows temperature dependences of n_e and μ_H , respectively, for the anatase TaON thin film fabricated at $T_S = 800$ °C. n_e was almost constant at $\sim 3.7 \times 10^{19} \text{ cm}^{-3}$ irrespective of temperature, indicating that the anatase TaON film is categorized as a degenerated semiconductor. Remarkably, μ_H at 300 K was as high as $\sim 17 \text{ cm}^2 \text{ V}^{-1} \text{ s}^{-1}$, which is comparable to that of anatase TiO_2 single crystal,⁸ namely, $\sim 17 \text{ cm}^2 \text{ V}^{-1} \text{ s}^{-1}$. However, μ_H was almost temperature-independent in the whole temperature range ($\sim 20 \text{ cm}^2 \text{ V}^{-1} \text{ s}^{-1}$), in sharp contrast to the anatase TiO_2 single crystal, in which μ_H is substantially enhanced at low temperatures where electron–phonon scattering is suppressed. Although the mechanism of the temperature independent μ_H in anatase TaON has not been

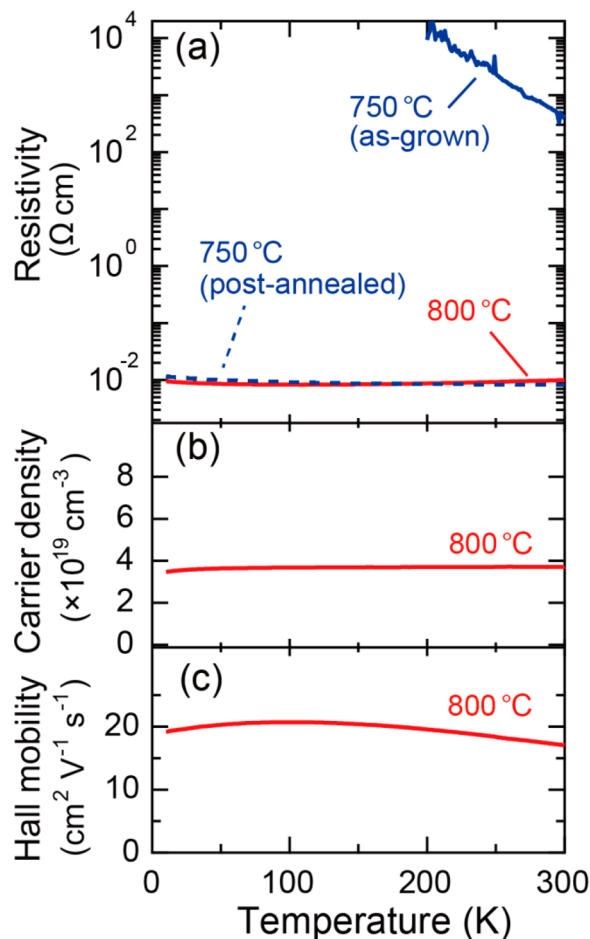


Figure 4. (a) Resistivity of anatase TaON epitaxial thin films plotted as functions of temperature. The dashed lines represent the data of the film grown at 750 °C and successively annealed at 800 °C under base pressure in the growth chamber. The resistivity of the film grown at 750 °C (as-grown) was measured by a two-probe method due to the high resistance. (b) Carrier density and (c) Hall mobility of the films grown at 800 °C plotted as functions of temperature.

fully understood yet, it is likely that the suppression of electron–phonon scattering at low temperatures is masked by predominant impurity scattering because the present films contain certain amounts of defects, such as anion vacancies and/or off-stoichiometry. Another possible explanation is that the electric transport is dominated by grain boundary scattering^{24–26} caused by planar defects observed in the TEM images. Even in the case of anatase TiO_2 , reduced samples with a high carrier density on the order of 10^{19} cm^{-3} , i.e., with a large number of oxygen vacancies, show similar suppression of μ_H at low temperatures.¹³ On the other hand, Nb-doped TiO_2 films exhibit much higher mobility than the reduced ones,⁹ suggesting that μ_H of anatase TaON could be further enhanced by doping with an appropriate cation.

Optical Properties of Anatase TaON. Finally, the optical properties of anatase TaON thin films will be briefly mentioned. Figure 5 shows the optical constants of the anatase TaON film grown at $T_S = 750$ °C determined by spectroscopic ellipsometry. The optical extinction coefficient, k , showed an abrupt increase around 2.3 eV. Assuming that anatase TaON is an indirect bandgap semiconductor like anatase TiO_2 ¹³ and baddeleyite TaON,²⁷ E_g was determined to be 2.37 eV from the $(\alpha h\nu)^{1/2}$ vs $h\nu$ plot (inset of Figure 5), where the absorption

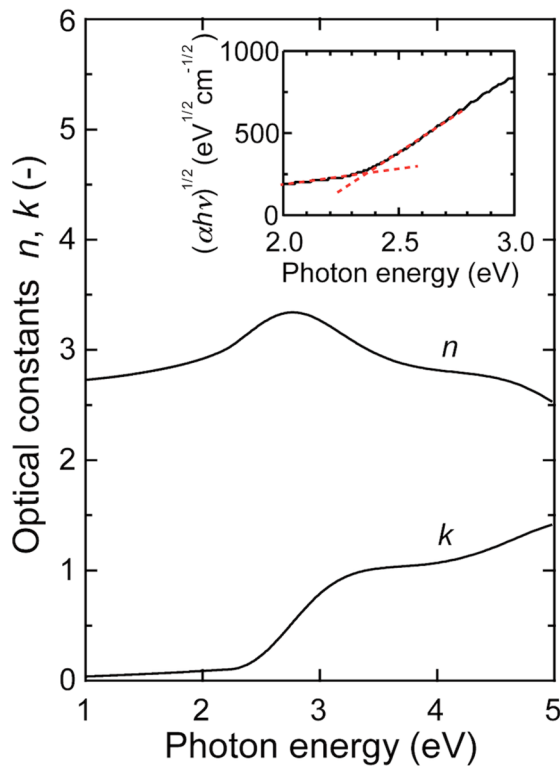


Figure 5. Refractive index n and extinction coefficient k of the anatase TaON thin film grown at $T_S = 750$ °C. (Inset) Optical bandgap of the anatase TaON thin film determined under an assumption that anatase TaON is an indirect transition semiconductor.

coefficient α was calculated from k ($\alpha = 4\pi k\lambda^{-1}$). This E_g value is comparable to those reported for anatase $Mg_{0.05}Ta_{0.95}O_{1.15}N_{0.85}$ (2.2 eV)¹⁷ and $Sc_{0.15}Ta_{0.85}O_{1.3}N_{0.7}$ (2.54 eV).¹⁸ The slight differences in the E_g values might be due to the difference in anion compositions or in lattice parameters. The refractive index, n , was approximately 3.0 in the visible light region, which is larger than that of Ta_2O_5 (~2.16)²⁸ and anatase TiO_2 (2.5–2.9)¹² in the same region. The higher n is explained by the stronger covalency of the Ta–N bond than Ta–O or Ti–O bonds, which tends to increase the polarizability.²⁹

CONCLUSION

Phase-pure anatase TaON thin films were epitaxially synthesized on lattice-matched single crystalline substrates by using NPA-PLD. A high growth temperature and a balanced supply of oxygen and nitrogen are crucial for obtaining high-quality anatase TaON thin films. Electrical transport measurements revealed that the anatase TaON film grown at $T_S = 800$ °C or reduced by vacuum annealing exhibited good n -type conduction with a resistivity, ρ , of $\sim 10^{-2}$ Ω cm and degenerated semiconducting behavior. The μ_H of ~ 17 cm² V⁻¹ s⁻¹ at 300 K is rather high for a d -electron based semiconductor and is comparable to that of anatase TiO_2 . The anatase TaON thin films exhibited E_g of 2.37 eV and n of ~ 3.0 in the visible region. The high μ_H as well as widely controllable conductivity show the potential of anatase TaON as an n -type semiconductor. Development of effective dopants will be a key to improving the transport properties of anatase TaON. Our results also demonstrated that epitaxial growth of thin films is a very promising approach for investigating the physical properties of

transition metal oxynitrides, which have been scarcely examined so far due to the difficulty in synthesizing single crystals.

AUTHOR INFORMATION

Corresponding Author

*E-mail: hirose@chem.s.u-tokyo.ac.jp.

Notes

The authors declare no competing financial interest.

ACKNOWLEDGMENTS

The authors thank Prof. Katsuyuki Fukutani, Mr. Seiji Ito, and Mr. Akira Morita of the University of Tokyo and Dr. Daiichiro Sekiba and Dr. Hiroshi Naramoto of the University of Tsukuba for their assistance in the NRA measurements. This study was supported by the Ministry of Education, Culture, Sports, Science and Technology (MEXT), Japan, as part of KAKENHI No. 24760005. A part of this work was conducted in the Research Hub for Advanced Nano Characterization, at The University of Tokyo, supported by MEXT, Japan.

REFERENCES

- (1) Guenther, E.; Jansen, M. *Mater. Res. Bull.* **2001**, *36*, 1399.
- (2) Kasahara, A.; Nukumizu, K.; Takata, T.; Kondo, J. N.; Hara, M.; Kobayashi, H.; Domen, K. *J. Phys. Chem. B* **2003**, *107*, 791.
- (3) Maeda, K.; Teramura, K.; Lu, D.; Takata, T.; Saito, N.; Inoue, Y.; Domen, K. *Nature* **2006**, *440*, 295.
- (4) Fuertes, A. *J. Mater. Chem.* **2012**, *22*, 3293.
- (5) Ye, Y.; Lim, R.; White, J. M. *J. Appl. Phys.* **2009**, *106*, 074512.
- (6) Kim, H.-S.; Jeon, S. H.; Park, J. S.; Kim, T. S.; Son, K. S.; Seon, J.-B.; Seo, S.-J.; Kim, S.-J.; Lee, E.; Chung, J. G.; Lee, H.; Han, S.; Ryu, M.; Lee, S. Y.; Kim, K. *Sci. Rep.* **2013**, *3*, 1459.
- (7) Yang, M.; Oró-Solé, J.; Kusmartseva, A.; Fuertes, A.; Attfield, J. P. *J. Am. Chem. Soc.* **2010**, *132*, 4822.
- (8) Forro, L.; Chauvet, O.; Emin, D.; Zuppiroli, L.; Berger, H.; Lévy, F. *J. Appl. Phys.* **1994**, *75*, 633.
- (9) Furubayashi, Y.; Hitosugi, T.; Yamamoto, Y.; Inaba, K.; Kinoda, G.; Hirose, Y.; Shimada, T.; Hasegawa, T. *Appl. Phys. Lett.* **2005**, *86*, 252101.
- (10) Hitosugi, T.; Furubayashi, Y.; Ueda, A.; Itabashi, K.; Inaba, K.; Hirose, Y.; Kinoda, G.; Yamamoto, Y.; Shimada, T.; Hasegawa, T. *Jpn. J. Appl. Phys.* **2005**, *44*, L1063.
- (11) Takeuchi, U.; Chikamatsu, A.; Hitosugi, T.; Kumigashira, H.; Oshima, M.; Hirose, Y.; Shimada, T.; Hasegawa, T. *J. Appl. Phys.* **2010**, *107*, 023705.
- (12) Mohri, S.; Hirose, Y.; Nakao, S.; Yamada, N.; Shimada, T.; Hasegawa, T. *J. Appl. Phys.* **2012**, *111*, 093528.
- (13) Tang, H.; Prasad, K.; Sanjinès, R.; Schmid, P. E.; Lévy, F. *J. Appl. Phys.* **1994**, *75*, 2042.
- (14) Matsumoto, Y.; Murakami, M.; Shono, T.; Hasegawa, T.; Fukumura, T.; Kawasaki, M.; Ahmet, P.; Chikyow, T.; Koshihara, S.; Koinuma, H. *Science* **2001**, *291*, 854.
- (15) Katayama, M.; Ikesaka, S.; Kuwano, J.; Koinuma, H.; Matsumoto, Y. *Appl. Phys. Lett.* **2008**, *92*, 132107.
- (16) Fujimoto, M.; Koyama, H.; Konagai, M.; Hosoi, Y.; Ishihara, K.; Ohnishi, S.; Awaya, N. *Appl. Phys. Lett.* **2006**, *89*, 223509.
- (17) Schilling, H.; Lerch, M.; Börger, A.; Becker, K.-D.; Wolff, H.; Dronskowski, R.; Bredow, T.; Tovar, M.; Baehtz, C. *J. Solid State Chem.* **2006**, *179*, 2416.
- (18) Stork, A.; Schilling, H.; Wessel, C.; Wolff, H.; Börger, A.; Baehtz, C.; Becker, K.-D.; Dronskowski, R.; Lerch, M. *J. Solid State Chem.* **2010**, *183*, 2051.
- (19) Schilling, H.; Stork, A.; Irran, E.; Wolff, H.; Bredow, T.; Dronskowski, R.; Lerch, M. *Angew. Chem., Int. Ed. Engl.* **2007**, *46*, 2931.
- (20) Bredow, T.; Lumey, M.-W.; Dronskowski, R.; Schilling, H.; Pickardt, J.; Lerch, M. *Z. Anorg. Allg. Chem.* **2006**, *632*, 1157.

- (21) van der Pauw, L. J. *Philips Res. Repts.* **1958**, *13*, 1.
(22) Jellison, G. E.; Modine, F. A. *Appl. Phys. Lett.* **1996**, *69*, 371.
(23) Miao, L.; Tanemura, S.; Jin, P.; Kaneko, K.; Terai, A.; Nabatova-Gabain, N. *J. Cryst. Growth* **2003**, *254*, 100.
(24) Seto, J. Y. W. *J. Appl. Phys.* **1975**, *46*, 5247.
(25) Furubayashi, Y.; Yamada, N.; Hirose, Y.; Yamamoto, Y.; Otani, M.; Hitosugi, T.; Shimada, T.; Hasegawa, T. *J. Appl. Phys.* **2007**, *101*, 093705.
(26) Minami, T. *Thin Solid Films* **2008**, *516*, 5822.
(27) Fang, C. M.; Orhan, E.; de Wijs, G. A.; Hintzen, H. T.; de Groot, R. A.; Marchand, R.; Saillard, J.-Y.; de With, G. *J. Mater. Chem.* **2001**, *11*, 1248.
(28) Kato, K.; Toyota, H.; Jin, Y.; Ono, T. *Vacuum* **2009**, *83*, 592.
(29) Pan, S. S.; Zhang, Y. X.; Teng, X. M.; Li, G. H.; Li, L. *J. Appl. Phys.* **2008**, *103*, 093103.